Catena 120 (2014) 164–176

Contents lists available at ScienceDirect

Catena

journal homepage: www.elsevier.com/locate/catena

Patterns of topographic change in sub-humid badlands determined by high resolution multi-temporal topographic surveys

D. Vericat [a,b,c,*], M.W. Smith [d], J. Brasington [e]

[a] Fluvial Dynamics Research Group (RIUS), Department of Environment and Soil Sciences, University of Lleida, E-25198, Lleida, Catalonia, Spain
[b] Forestry and Technology Centre of Catalonia, 25280 Solsona, Catalonia, Spain
[c] Institute of Geography and Earth Sciences, Aberystwyth University, SY23 3DB, Wales, UK
[d] School of Geography, University of Leeds, Leeds, LS2 9JT, UK
[e] School of Geography, Queen Mary, University of London, Mile End, London, E1 4NS, UK

ARTICLE INFO

Article history:
Received 19 September 2013
Received in revised form 7 April 2014
Accepted 11 April 2014
Available online 20 May 2014

Keywords:
Badlands
Terrestrial Laser Scanning
Topographic change
Roughness
Event-scale
Annual-scale

ABSTRACT

Badlands are highly erodible landscapes with sparse vegetation and rapid runoff responses. Badland surfaces experience high erosion rates that may have a direct and marked influence on river channel networks and catchment scale sediment budgets. Erosion rates from badlands have been widely estimated by discrete observations of topographic change measured by erosion pins or profile meters. Recent developments in survey instrumentation provide the opportunity to build high-resolution topographic models over multiple spatial scales at sub-centimeter accuracy. In this paper we demonstrate how reliable estimates of topographic variables and temporal change can be derived for badlands by repeat Terrestrial Laser Scanning (TLS) surveys undertaken at multiple temporal (event to annual) scales.

A total of seven TLS-surveys were obtained in an experimental sub-humid badland located in the Central Pyrenees. Data analyses were conducted on two temporal scales: (a) five rainfall events and (b) three long term (spaced over an annual cycle) scales. Our results show a clear erosional pattern for most of the badland at the annual scale (i.e. annual net change at around -6 cm yr^{-1}). Aspect, surface roughness and slope were significant predictors of topographic change, although the sign and magnitude of the change differed at the event scale. Net topographic change at the event scale varied from -1.8 to 1.4 cm. Although these patterns could be also affected by swell-shrink processes, surface roughness was more important at controlling badland geomorphological processes at the event-scale than the annual scale. Our observations suggest that longer-term studies may underestimate the importance of surface roughness as a control on badland geomorphology. At the annual scale the effect of aspect in the sign of the topographic change was removed and slope becomes more important. Erosion proved to be dominant on slopes higher than 100%. Overall, the results indicate that coupling of appropriately-scaled spatial and temporal data is critical to understand topographic changes and their drivers on badlands. Although the approach outlined in this paper was only applied to a relatively small area, with careful survey design and application of new survey technology, it could readily be upscaled to cover entire badland systems. Such surveys would permit detailed analysis of controls of sedimentological connectivity across badlands and their influence on channel networks and catchment sediment budgets.

1. Introduction

1.1. Badlands: complex interactions in highly erodible landscapes

Badlands are dissected landscapes with sparse or absent vegetation, characterized by unconsolidated sediments being useless for agriculture (Bryan and Yair, 1982; Fairbridge, 1968; Gallart et al., 2013; Howard, 1994). Badland areas demonstrate rapid runoff response and, due to the high erodibility, high erosion rates which, despite occupying relatively small areas, can make disproportionate contributions to catchment scale sediment budgets (e.g. García-Ruiz et al., 2008; López-Tarazón et al., 2012). The amount of sediment eroded from badlands and transferred to channel networks may have negative effects not just in the main channel network (e.g. channel bed clogging; Buendia et al., 2013) but also off-site consequences (e.g. reservoir siltation and loss of capacity; Avendaño et al., 2000; Palau, 1998).

Rapidly evolving badlands have been used as a testing ground for geomorphic concepts and hypotheses, under the assumption that they represent comparatively simple 'model landscapes' or natural analogues of morphologically similar but larger erosional landforms (Schumm, 1956). Badlands are then considered field laboratories

* Corresponding author at: Fluvial Dynamics Research Group (RIUS), Department of Environment and Soil Sciences, University of Lleida, E-25198, Lleida, Catalonia, Spain. Tel.: +34 973 003735; fax: +34 973 702613.
E-mail address: dvericat@macs.udl.cat (D. Vericat).

http://dx.doi.org/10.1016/j.catena.2014.04.012
0341-8162/

(as per Kasanin-Grubin, 2013). Yet, badlands experience regular rainsplash, sheetflow, rill, pipe and gully erosion, forming heavily dissected landscapes. Gravity driven processes of creep and mass movement along with freeze-thaw activity also contribute to the observed erosion rates (Nadal-Romero et al., 2007; Vergari et al., 2013). The combined erosional response is a complex function of an assemblage of geomorphological processes operating at distinct spatial and temporal scales.

Although diverse in their origins, climatic setting and development, badlands form frequently on unconsolidated sediments that are especially vulnerable to erosion, particularly marls, clays and shales. Considerable spatial and temporal variability in runoff generation and erosion processes is reported in badland areas (e.g. Kuhn and Yair, 2004; Solé-Benet et al., 1997) with direct influence on the transfer of fine sediments across channel networks (e.g. Francke et al., 2008; López-Tarazón et al., 2011). However, in some cases, the rapid erosion rates preclude soil development and establishment of extensive plant cover. Spatial patterns in erosion rates arise from lithological controls (Bryan and Yair, 1982; Cerdà, 2002), regolith surface characteristics (Regüés and Gallart, 2004), aspect (Alexander et al., 1994; Yair and Lavee, 1985), vegetation or biological crusts (Lázaro et al., 2008), soil moisture (Cantón et al., 2004), soil physical and chemical properties including mineralogy (Faulkner et al., 2000; Imeson et al., 1982; Kasanin-Grubin, 2013) and surface roughness (Solé-Benet et al., 1997). The episodic nature of sediment transport events has been reported as a function of rainfall intensity and duration (Torri et al., 1999) and antecedent conditions (Descroix and Claude, 2002). Connectivity of hydrological and sedimentological systems also determines broader scale badland morphology and the efficiency with which eroded sediment is exported from badland systems (Faulkner, 2008; Godfrey et al., 2008). The effects of different surface properties and their interactions at multiple temporal and spatial scales remains of current interest to the research community (e.g. Cantón et al., 2011).

1.2. Assessing topographic change in badlands

The study of erosion rates on badlands has gained momentum in recent years (Gallart et al., 2013). A wide range of badland erosion rates has been reported (Clarke and Rendell, 2010; Nadal-Romero et al., 2011, 2013; Wainwright and Brazier, 2011). Comparison of values is problematic as observed erosion rates are influenced by both the measurement technique and the spatial and temporal scale of measurement (Sirvent et al., 1997). Measurements may also be affected by swell-shrink processes controlled by moisture and temperature. Therefore, these conditions need to be equivalent between survey periods in order to obtain topographic changes directly related to erosional and depositional processes. Erosion pins are used commonly to provide direct point measurements of surface lowering or change (e.g. Ciccacci et al., 2008; Clarke and Rendell, 2006; Della Seta et al., 2009; Francke, 2009; Schumm, 1956; Sirvent et al., 1997), demonstrating considerable spatial variability according to the specific geomorphic setting and surface properties. Reported erosion rates range from <1 mm yr^{-1} to 80 mm yr^{-1} in eroding rills during a single storm event (Cantón et al., 2001). Additionally, sediment collected from bounded plots (e.g. Lázaro et al., 2008) and at catchment outlets (e.g. Cantón et al., 2001) have been used to calculate contemporary denudation rates in such landscapes. Large differences in erosion rates for the same area using different methods have been reported (Desir and Marín, 2007). Recently, Ballesteros-Cánovas et al. (2013) provided a review of dendrogeomorphological methods applied to erosion measurements in badlands landscapes.

The multitude of geomorphological processes and controlling factors in operation creates a major sampling problem, limiting the representativeness of at-a-point erosion pin sampling in the face of reported spatial variability. Extrapolation from experimental plots is problematic (Boardman, 2006; Boix-Fayos et al., 2006), while sampling at the catchment outlet provides no understanding of spatial and temporal patterns of processes. Moreover, substantial monitoring errors arise in badland areas due to hyper-concentrated flows and high erosion rates filling sediment traps. Sampling uncertainties associated to the heterogeneous characteristics of sediments and the variability of suspended sediment concentrations during flood events have been reported by Regüés and Nadal-Romero (2013). Inverse estimation of sediment transport patterns and rates from analysis of morphological dynamics (Ashmore and Church, 1998; Brasington and Smart, 2003) presents a viable alternative to estimate topographic changes, to identify patterns, to assess their controls and to understand their dynamics over multiple temporal scales.

1.3. Terrestrial laser scanning: opportunities and challenges in the study of badland evolution

Volumetric changes in badlands have been largely estimated from detailed surveys using profile meters (e.g. Descroix and Claude, 2002; Sirvent et al., 1997). Advances in survey technologies offer a compromise of both detailed and relatively extensive high-resolution surveys using differential Global Positioning Systems (Brasington et al., 2000; Fuller and Marden, 2011), airborne LiDAR (Liu, 2008; see Bretar et al., 2009; Lopez-Saez et al., 2011; Thommeret et al., 2010 for specific applications in badlands studies) or Terrestrial Laser Scanning (TLS) (Brasington et al., 2012; Lucía et al., 2011a, 2011b; Milan et al., 2007; Williams et al., 2011). TLS has the advantage of being a non-contact survey method avoiding unnecessary disturbance to extremely erodible badland surfaces, obtaining topographic models at unprecedented accuracy and density. The density of these point clouds allows modelling landscapes at the grain scale, being able not just to extract topography but also some of the characteristics of these such as surface roughness (see Brasington et al., 2012 in case of fluvial environments, and Eitel et al., 2011 for an experimental study in rangelands).

Differencing TLS-based digital elevation models (DEMs) offers robust estimation of space-time averaged volumetric changes that can be implemented at a variety of scales. Moreover, the spatial distribution of erosional and depositional processes can be examined and the relative importance of individual erosional processes and controlling factors elucidated. However, since estimated volumetric changes are strongly sensitive to the integration time used in their calculation, the survey revisit time will determine whether short term fluctuations in surface form can be distinguished from longer term trends. Previously, progress with TLS has been hampered by a lack of efficient data post-processing strategies to derive relevant data products to study landscape topographic characteristics and evolution at large scales. Recently, Brasington et al. (2012) presented an open source geospatial toolkit, ToPCAT (topographic point cloud analysis toolkit), which provides a framework to analyse very large TLS data sets and generate terrain data (i.e. DEMs) suitable for change detection at multiple spatial scales. However, distributed sediment budget estimations derived from multi-temporal surveys are sensitive to the terrain data quality (as reported by Brasington et al., 2000). A threshold minimum level of detection must be calculated to distinguish real geomorphic changes from noise (Brasington et al., 2003; Lane and Chandler, 2003; Wheaton et al., 2010). Yet DEM uncertainty is itself spatially variable which requires a distributed approach to propagating uncertainty to elevation difference models (Wheaton et al., 2010) and provide a real estimate of volumetric changes. Here we present a pilot study to demonstrate a workflow for extracting reliable topographic change from TLS data. The aim of this paper is to examine the spatial and temporal variability of erosion and deposition patterns in a highly erodible sub-humid badland area using high spatial and temporal resolution repeat TLS surveys. Erosional-depositional processes and their controlling topographic and meteorological factors are investigated over a number of event-scale monitoring periods. Finally, the effect of spatial and temporal scale of data collection on estimated topographic changes rates is critically examined.

2. Study site

This study was conducted in an area of badlands located in the Villacarli catchment (42 km^2; Fig. 1A). The River Villacarli is one of the largest tributaries of the Isábena catchment (445 km^2, Ebro Catchment, Central Pyrenees, Iberian Peninsula). López-Tarazón et al. (2012) reported the highly dynamic sedimentological character of the Isábena catchment. The altitude varies from more than 2700 meters in the headwaters, down to 445 meters in the lowermost course of the river. The catchment has a Continental Mediterranean climate with a high spatial variability in annual rainfall; oscillating between 450 and 1600 mm yr^{-1}, with a mean value of around 770 mm yr^{-1}. Mean daily temperature ranges from almost 3 °C in winter to up to 19 °C in summer. Freezing temperatures (considered below 0 °C) are often reached (and preserved) in winter as can be seen later in this study. Northern parts of the catchment are composed of highly erodible materials (marls and sandstones from the Paleogene and Cretaceous). These materials are vulnerable to the formation of badlands. Though the extension of the badlands is relatively small when compared to the whole Isábena catchment (<1%), these areas have been shown to be the major source of sediment in the catchment outlet (Alatorre et al., 2010; Fargas et al., 1997; Francke et al., 2008).

Although these features are well-connected to the main channel network, sediment delivery from badlands is highly variable because of the complex interactions between landscape and climate variables. As a consequence, the main channel of the River Isábena suffers annual cycles of fine material sedimentation and erosion (López-Tarazón et al., 2011). These cycles regulate the amount of fine sediment availability that, in turn, control suspended sediment concentrations downstream at the outlet of the basin. For instance, during baseflows and with a situation of high sediment availability, concentrations up to 1 g l^{-1} are observed in the outlet of the catchment, which may reach values close to 300 g l^{-1} during flood events (López-Tarazón et al., 2011, 2012). Within this context, studying the complex spatial and temporal patterns of sediment export from badlands and their drivers remains a key component of understanding sediment production in catchments draining high erodible surfaces such as badlands.

Almost 60% of the total badland area of the Isábena catchment is concentrated in the Villacrali sub-catchment, where ~6% of the total area is occupied by badlands. An experimental badland within this area has been selected to carry out this pilot study (Fig. 1B–C). The targeted badland has an area of 36 m^2, a maximum altitude of 996.2 meters a.s.l., and a relief of 7.5 m. The average slope is at around 100% (range of 16% — 250%). Median particle size (D_{50}) of the sediments is 0.0034 mm (i.e. silt), while largest materials (D_{95}) have a size at around 0.067 mm (very fine sand to coarse silt).

3. Methods

3.1. Data acquisition

The experimental badland (Fig. 1B) was surveyed 7 times between 2009 and 2010. The first scan was obtained in summer 2009

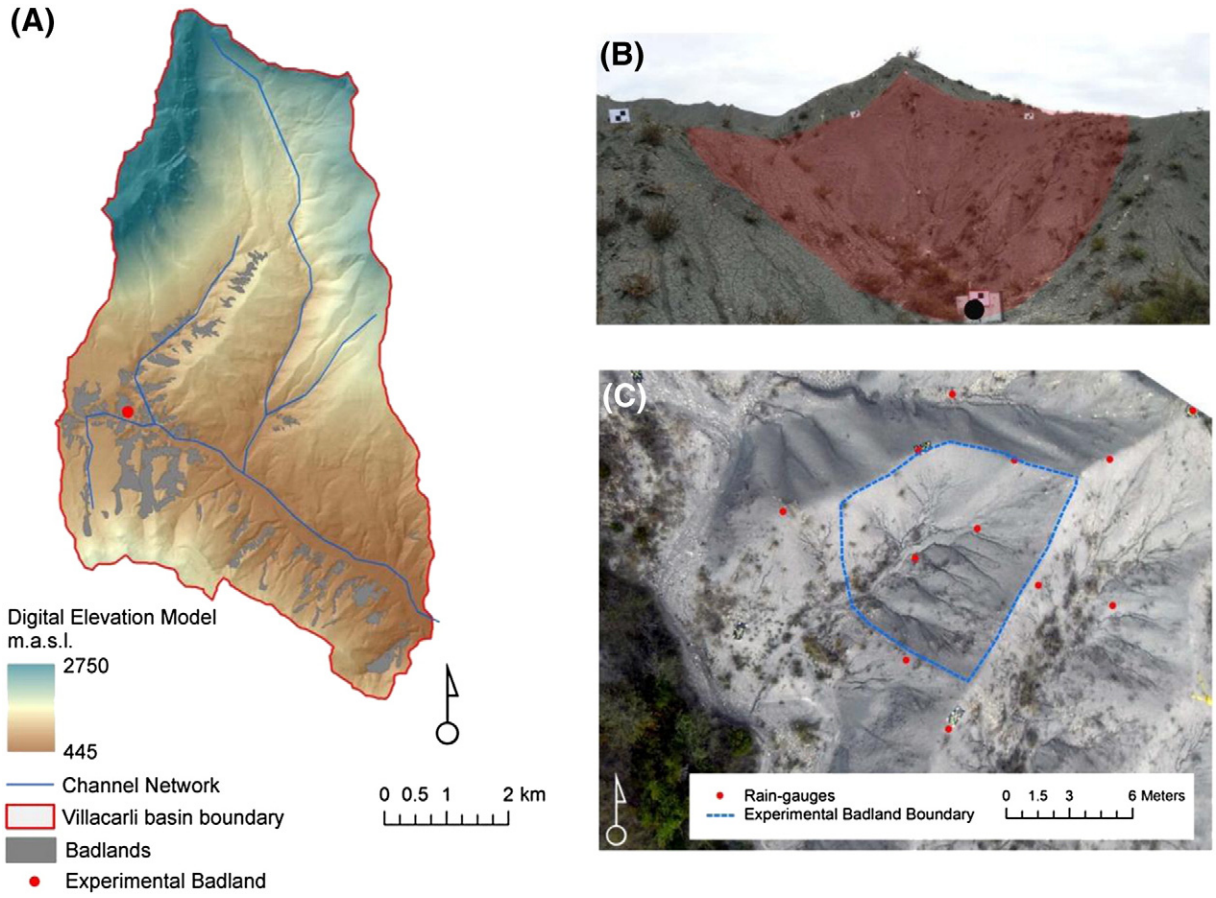

Fig. 1. Field site location. (A) Location of experimental badland within the Villacarli catchment; (B) Oblique imagery outlining experimental badland; (C) Aerial image detailing the boundary of the experimental badland and rain gauge network.

(28 August 2009) as part of a larger-scale survey using a Leica ScanStation (360° × 270° field-of-view, single-point range accuracy of 4 mm, beam spot size of 4 mm from 0–50 m range) from multiple station setups. A further six scans were obtained regularly following individual rainfall events between September and December 2010. These event-based scans were obtained using a Leica HDS2500 (40° × 40° field-of-view, single-point range accuracy of 4 mm, beam spot size of 6 mm from 0-50 m range) from a common single station setup at the outlet of the experimental badland.

TLS surveys were georeferenced to a geographic coordinate system (i.e. ED50) using primary and floating control networks. The coordinates of the 6 ground control points (GCPs) of the primary control network where obtained using a Leica Viva GS15 differential GPS and post-processed with RINEX data available at the Spanish National Geographic Institute (IGN) and the Aragon Territorial System of Information (SITAR). The 3d data quality (position and elevation) of all GCPs was sub-centimetre. The floating network of black and white TLS targets was mounted on tripods and was re-surveyed for each campaign using a reflectorless total station (Leica TCRP 1205), and registered to the fixed network control. The average TLS target 3d data quality after registration was 0.005 m (ranging from 0.0028 to 0.0072 m).

Rainfall was measured continuously using a network of 12 tipping-bucket rain gauges (Decagon ECRN-50) that record rainfall at 1 mm precision (see location in Fig. 1C) and logged the total rainfall in each 15 minute interval. Air temperature was also recorded every 15 minutes using a Trutrack sensor installed at the outlet of the badland. This sensor was positioned close to a sediment pit trap (highlighted in Fig. 1B). However, owing to the dynamic nature of these badlands, the sediment trap filled too rapidly within each event for sediment export to be monitored reliably. This issue emphasises the problematic nature of implementing conventional sediment transport measurement techniques at such dynamic locations.

3.2. Data post-processing

Georeferenced point clouds were fragmented by intensity to remove vegetation points (Fig. 2A). Point densities were unified through application of the open source ToPCAT algorithm (Brasington et al., 2012; Rychkov et al., 2012) creating multi-resolution gridded ($x_i - y_i$) terrain products (Fig. 2B). Sub-grid scale statistical measures were also calculated. Multiple grid sizes were applied in the particular case of this study (0.05, 0.10, 0.20, 0.50 and 1 m grid sizes), though point densities

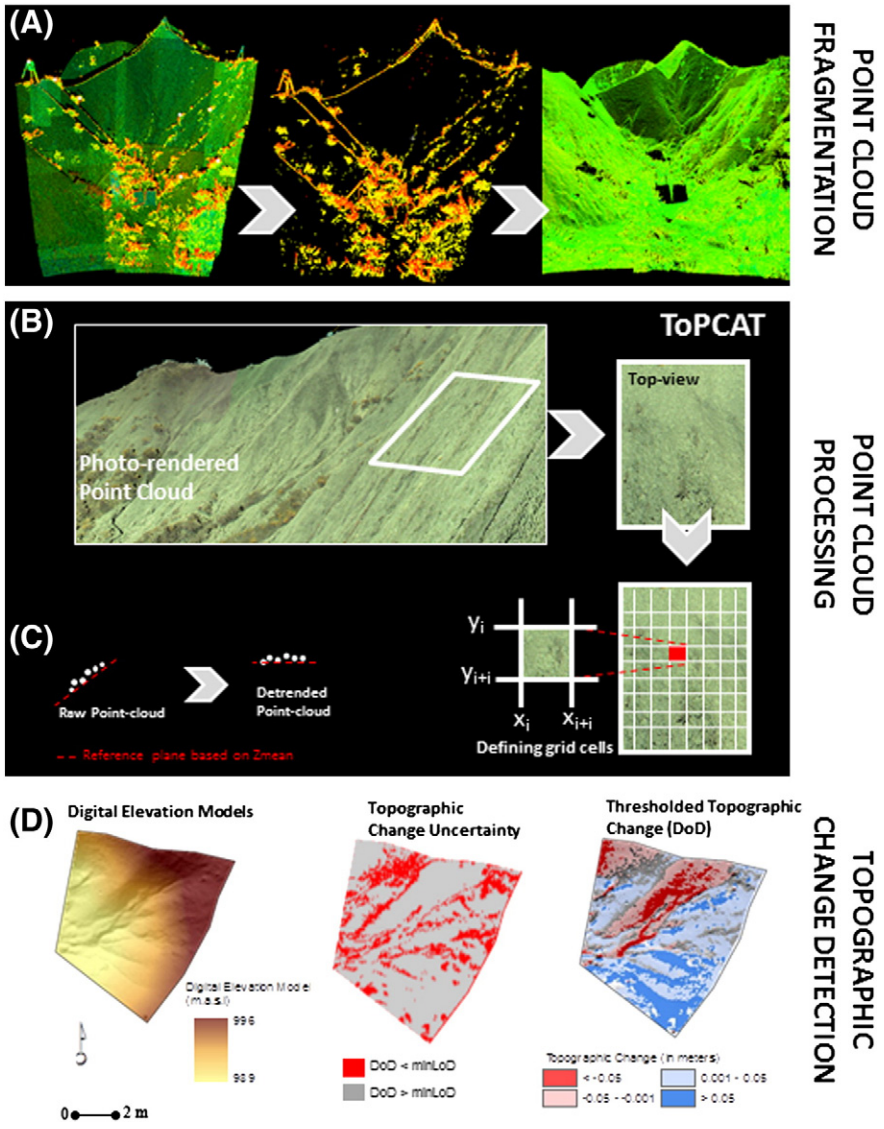

Fig. 2. Post-processing methods applied to georeferenced point clouds. (A) Intensity-based filtering of vegetation; (B) unification of point cloud density; (C) extraction of sub-grid statistics; (D) production of thresholded DEMs of Difference (DoDs) to distinguish real topographic changes from DEM uncertainty.

Table 1
Summary of meteorological data recorded during the monitoring period. Summary data are presented for both event-scale intervals (ES1–ES5) and overlapping longer term intervals (LT1-LT3).

Period	Monitoring interval	Number of days	Total rainfall (mm)	Maximum rainfall (mm/15')	Mean temperature (ºC)	Days, T < 0 ºC
Event Scale 1 (ES1)	01 Sep. 2010–16 Sep. 2010	15	70.0	22.3	18.3	0.0
Event Scale 2 (ES2)	16 Sep. 2010–08 Oct. 2010	22	59.6	4.0	13.8	0.0
Event Scale 3 (ES3)	8 Oct. 2010–16 Oct. 2010	8	52.5	3.7	12.9	0.0
Event Scale 4 (ES4)	16 Oct. 2010–17 Nov. 2010	32	78.0	2.5	6.9	11
Event Scale 5 (ES5)	17 Nov. 2010–29 Dec. 2010	42	108.0	2.5	1.1	32
Long Term Scale 1 (LT1)	01 Sep. 2010–29 Dec. 2010	119	368.2	22.3	10.7	43
Long Term Scale 2 (LT2)	28 Aug. 2009–01 Sep. 2010	369	690.2	13.5	-	-
Long Term Scale 3 (LT3)	28 Aug. 2009–29 Dec. 2010	488	1058.4	22.3	-	-

of the raw data were much higher. This yielded a large number of points per grid cell, providing the required data to analyse the topographic complexity within each cell (e.g. the maximum, minimum and mean of the elevations; standard deviation of the elevations). The minimum point elevation within each grid cell (Z_{min}) was used to develop a terrain model (DEM) of the badland surface at each time interval. A neighbourhood triangular tessellation based on the mean elevation in each grid (Z_{mean}) was used to reconstruct the local surface and detrend all points within the central grid cell (Fig. 2C). The standard deviation of the detrended points was then calculated for each grid cell separately. The detrended standard deviation of elevations is considered a proxy for sub-grid roughness.

Changes between each sampling interval were calculated by subtracting the old DEM from the new DEM to create a DEM of Difference (DoD). Negative results indicate erosion while positive sedimentation. To distinguish real topographic change from errors in the individual topographic models, a threshold minimum level of detection was calculated and applied (following Brasington et al., 2000, 2003). The analyses presented in the open source algorithm DoD3 (Wheaton et al., 2010) were performed although in the particular case of this study a single source of uncertainty was considered as explained below.

The error in the final DoD (or minimum level of detection for real topographic change, minLoD) was calculated from errors in each DEM as:

$$minLoD = t\left[\varepsilon_{DEM1}^2 + \varepsilon_{DEM2}^2\right]^{0.5}$$

where t is the critical t value for a given confidence interval and ε_{DEMi} the errors associated to the new ($i = 1$) and old ($i = 2$) DEMs. Using the 90% confidence interval, $t = 1.65$. From the sub-grid roughness parameterisations extracted from ToPCAT, the detrended standard deviation of elevations (i.e. sub-grid roughness) was applied to represent ε_{DEMi}. This provided a spatially-variable minimum level of detection based upon local topographic roughness. Thus, small topographic changes would be undetectable on rough surfaces but could be considered significant over smoother surfaces where sub-grid topographic variability is small. Calculated topographic changes below the minLoD were filtered out of each DoD (Fig. 2D). To examine the effect of grid size on calculated changes, this process was repeated for selected intervals at multiple grid sizes (0.05, 0.10, 0.20, 0.50 and 1 m grid size).

Six topographic variables were extracted from the DEMs to investigate potential topographic drivers of the spatial pattern of change

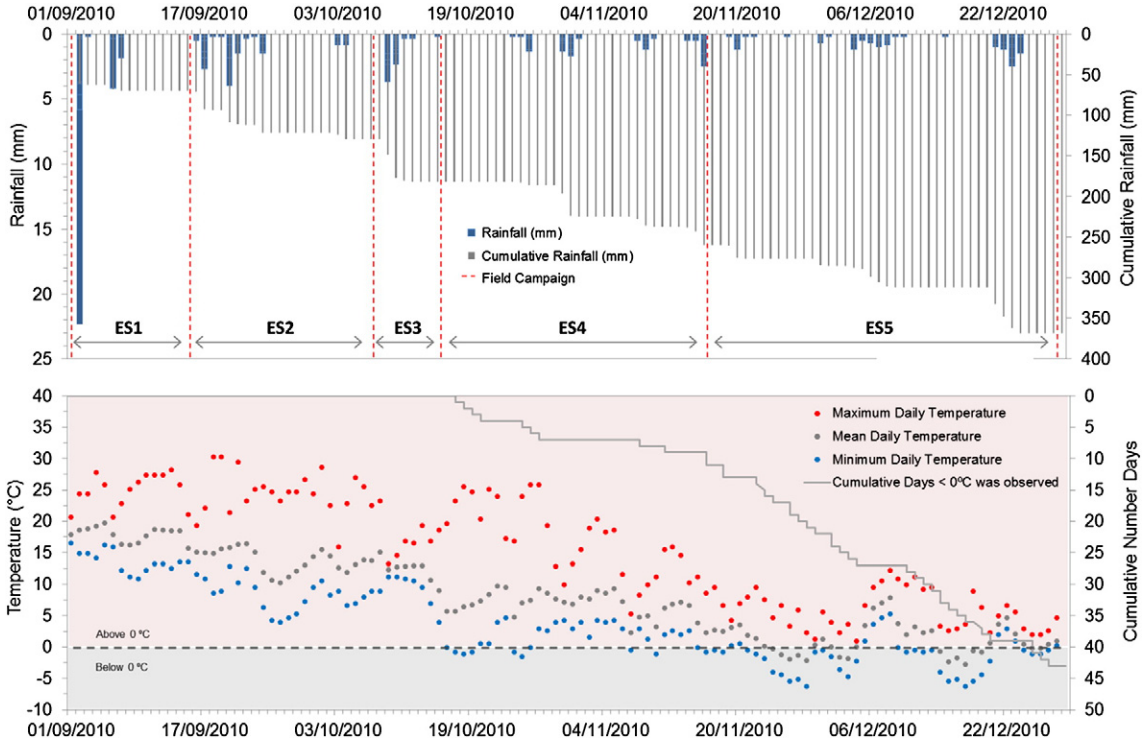

Fig. 3. Meteorological data during the intensive survey period. Daily total rainfall amounts and cumulative rainfall are presented, while maximum, mean and minimum daily temperature measurements are shown to demonstrate the variation of daily temperature range. The bottom plot also represents the cumulative number of days reaching temperatures lower than 0 °C. Survey dates (dashed red line) and analysed periods (between arrows) are also indicated. Dashed grey line in the bottom diagram indicates the freezing threshold (i.e. 0 °C).

(erosion and deposition). These were: (i) the upslope catchment area of each cell (m^2); (ii) slope of each grid cell (%); (iii) mean slope of all upstream cells contributing to each cell (%); (iv) topographic wetness index of each cell calculated as $\ln(A/\tan\beta)$ where A is upslope area and β is local slope; (v) local surface roughness (in m) parameterised using the detrended standard deviation of the elevations within each grid cell; and (vi) aspect. The DEM from the start of each survey interval was used to calculate topographic variables.

Additionally, five meteorological variables were calculated to determine the meteorological influence on observed temporal variability of erosion and deposition for event-scale survey intervals. Rainfall data were filtered in order to remove isolated cases of malfunctioning rain gauges. A single rainfall record was established by averaging the 15-minunte recording data from all working gauges. Final calculated variables were: (i) total rainfall and (ii) maximum rainfall intensity between TLS surveys, (iii) the mean temperature of each survey interval, (iv) the temperature amplitude, and (v) the number of days below freezing (i.e. 0 °C; calculated as the number of days in which at least one value below 0 °C was registered in the 15-minute interval data set).

Pearson correlation coefficients and circular statistics in the particular case of aspect (Berens, 2009) were calculated to assess the influence of topographical and meteorological variables on topographic changes.

4. Results

Data analyses are conducted on two temporal scales: (a) five event-scale (hereafter ES; starting on September 1st 2010 and ending on December 29th 2010) and (b) three long term scale (hereafter LT; from 28th August 2009 to December 29th 2010). Dates and intervals are presented in Table 1, while sampling periods are graphically indicated in Fig. 3. The length of the event-scale survey intervals ranged from 42 days (ES5) to just 8 days (ES3). During this intensive survey period a total of 368 mm of rain fell in several discrete rainfall events (Fig. 3; Table 1). Maximum 15-minute intensity ranged from 22.30 mm to 2.50 mm (Fig. 3). Mean temperatures gradually decreased during the year with sub-zero temperatures recorded from the forth survey interval (ES4) onwards when daily temperature range also decreased substantially. By the final survey interval the mean temperature was just 1 °C (Fig. 3). Three long-term intervals are defined to study the effect of the temporal scale on topographic change estimates. The length of these periods ranges between 119 (LT1) and 488 (LT3) days. Meteorological variables for these intervals are presented in Table 1.

Results are structured in four sections. First, the spatial and temporal variability of topographic changes are described at multiple temporal scales (Section 4.1). Second, the effect of the topographic variables on the spatial patterns of erosion and deposition at the event-scale is

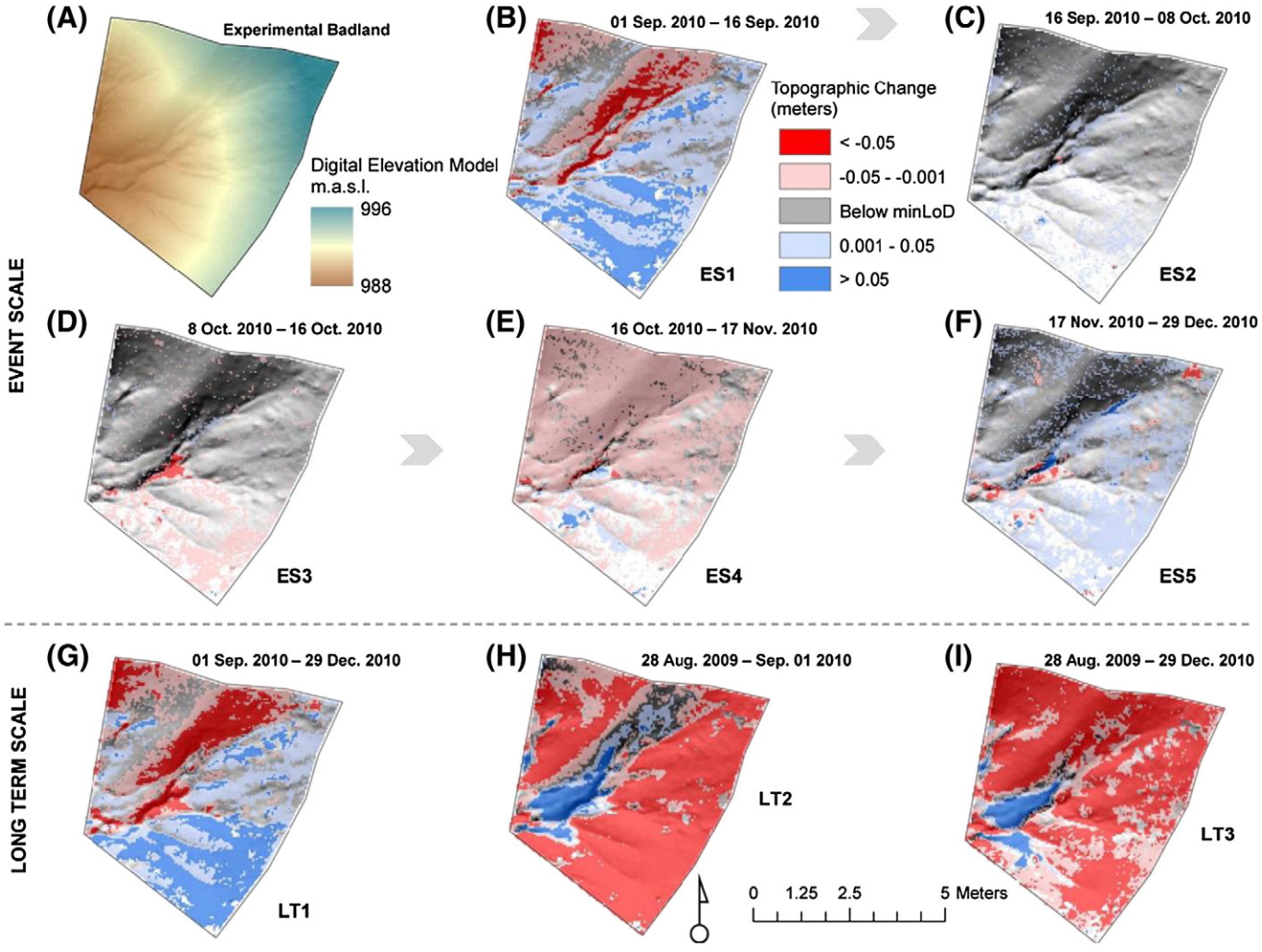

Fig. 4. Observed topographic changes in the experimental area. (A) DEM (50 mm grid size; 01 Sep. 2010); (B–F) Topographic changes observed at the event scale; (G–I) Long-term topographic changes observed over longer survey intervals. Where changes are below the minimum level of detection the underlying shaded DEM is visible.

Table 2
Summary of observed topographic changes for different survey intervals.

Period	Area above minLoD (m^2 and %)	Topographic change				
		Mean ± SD[a] Erosion[b] (m)	Erosion Area (m^2 and %[c])	Mean ± SD[a] Deposition[d] (m)	Deposition[d] Area (m^2 and %[b])	Balance ± SD[1] (m)
ES1	28.1 (77%)	−0.042 ± 0.023	9.4 (34%)	0.043 ± 0.021	18.7 (66%)	0.014 ± 0.046
ES2	4.6 (13%)	−0.027 ± 0.032	0.1 (0.7%)	0.010 ± 0.007	4.5 (99%)	0.009 ± 0.011
ES3	6.0 (17%)	−0.019 ± 0.022	5.3 (88%)	0.016 ± 0.015	0.7 (12%)	−0.015 ± 0.024
ES4	24.6 (67%)	−0.020 ± 0.008	23.4 (96%)	0.035 ± 0.027	1.2 (4%)	−0.018 ± 0.015
ES5	15.6 (43%)	−0.037 ± 0.023	1.8 (12%)	0.020 ± 0.013	13.8 (88%)	0.013 ± 0.023
LT1	27.8 (76%)	−0.049 ± 0.026	11.8 (42%)	0.050 ± 0.062	16.0 (58%)	0.008 ± 0.055
LT2	32.9 (90%)	−0.083 ± 0.036	28.6 (87%)	0.073 ± 0.057	4.3 (13%)	−0.062 ± 0.066
LT3	33.2 (91%)	−0.065 ± 0.025	30.8 (92%)	0.089 ± 0.061	2.5 (8%)	−0.054 ± 0.050

[a] ±SD refers to plus/minus the standard deviation of the calculated statistic.
[b] Erosion reflects elevation decrease during the survey interval which may actually be related to erosional or shrink processes.
[c] Percentage of the area above the minLoD.
[d] Deposition reflects elevation increases during the survey interval which may actually reflect both depositional and dilatation processes. See text for further discussion.

analysed (Section 4.2). Third, relationships between event-scale erosion and deposition and meteorological variables are investigated (Section 4.3). Finally, the effect of survey spatial and temporal scale on these results is assessed (Section 4.4).

4.1. Observed topographic changes

A DEM of the experimental badland is presented in Fig. 4A. To the north of the badland slopes are mostly south-facing, though there is a minor reversal of this trend as a subcatchment also drains this northern slope. This is most evident in the hillshade that can be seen in Fig. 4C. The southern slopes are north-facing and display several rills. A central drainage line runs from east to west with ~7 m graded change from the divide to the outlet. From the northern corner to the southern corner the range in elevations is approximately 3 m.

Observed topographic changes over different survey intervals are presented as thresholded DoDs from Fig. 4B–4I. Erosion and deposition values are summarised in Table 2. It should be noted that 'deposition or sedimentation' more accurately reflects elevation increases which may actually reflect both depositional and dilatation processes (swelling); while 'erosion' could also be attributed to shrink processes. Data on soil moisture and temperature is not available in order to verify that these conditions were equivalent between survey periods and, consequently, the effects of swell-shrink processes in the observed patterns cannot be directly distinguished. Between 1st September and 29th December 2010 the 6 repeat topographic surveys yielded 5 event-scale survey intervals (ES1–ES5; Fig. 4B–F). Despite being one of the shorter intervals, ES1 showed the largest and most variable topographic change. Fig. 4B highlights that the majority of the plot surface (77%) demonstrated significant change (i.e. DoD > minLoD). The spatial variability of these changes indicates two distinct zones: (i) erosion predominant on the south-facing slopes and (ii) an increase in elevation observed on the north-facing slopes. The dominant process in terms of areal extent was deposition (66% of the total area was above the minLoD). Net change was 0.014 m although the variability of erosion/deposition processes was extremely high as reflected in the high standard deviation (SD) of the thresholded DoDs (Table 2). Substantial erosion (<50 mm) was observed on the main drainage lines.

Subsequent event-scale survey intervals show substantially smaller topographic changes in magnitude and in extent. Only 13% of the surface was above the minLoD in ES2 with most of these changes being associated with deposition (99% of the area above minLoD) despite 60 mm of rain falling in this interval. Interestingly, although deposition is more extensive, the mean erosion rate was −0.027 m, almost three times higher the mean deposition rate (Table 2). Erosion is, however, mostly observed in ES3 both in extent (88% of the area) and in magnitude terms (mean erosion value of −0.019 m). This dominance provides a net change of −0.015 m. Erosion is concentrated in both on main drainage lines and on north-facing slopes, though the latter may simply be reversal of the swelling process observed in ES1 (Fig. 4).

ES4 was longer than previous intervals (~1 month) and displayed erosion over 67% of the badland surface with erosion concentrated in the main drainage lines. Erosion was the dominant process (96% of the area above the minLoD). A small zone of deposition is also evident on the north-facing slopes. The magnitude of the deposition in this zone is high (Table 2), yielding a mean deposition rate of 0.035 m, clearly higher than the mean erosion rate (−0.020 m). Finally, for ES5, the longest event-scale survey interval, 43% of the area is above the minLoD and most of this is associated with deposition (88% of the area). This period coincides with the highest total rainfall but the lowest rainfall intensity and the onset of freezing temperatures (Fig. 3 and Table 1). These conditions may reflect surface expansion due to freezing

Table 3
Pearson correlation coefficients between topographic variables and observed topographic change. Circular correlations presented for aspect. A positive change represents deposition during the survey period. Significant correlations ($p < 0.01$) are indicated with an asterisk while the strongest relationship for each survey period is also highlighted in bold. Numbers in parentheses in the roughness column are Pearson correlation coefficients for absolute topographic change.

Period	Aspect[a]	Upstream area (A)	TopographicWetness Index (TWI)	Slope (S)	Mean contributing slope (MCS)	Roughness (dSD)	Number of obs
ES1	**0.856***	0.063*	−0.024	0.014	0.071*	0.098* (0.149*)	10975
ES2	0.103*	0.094*	0.036	−0.046	0.043	0.242* (**0.687***)	1738
ES3	0.171*	−0.091*	0.078*	−0.267*	−0.052	−0.417* (**0.632***)	2323
ES4	**0.545***	0.096*	0.075*	−0.128*	−0.082*	0.067* (0.446*)	9592
ES5	0.183*	−0.028	0.125*	−0.005	0.018	−0.005 (**0.532***)	6081
LT1	**0.801***	−0.010	−0.005	0.017	0.092*	0.095* (0.173*)	10800
LT2	**0.544***	0.041*	0.096*	−0.289*	−0.391*	−0.208* (0.249*)	12664
LT3	0.180*	−0.020	0.061*	−0.363*	**−0.460***	−0.069* (0.105*)	12800

* $p < 0.01$.
[a] Circular statistics were performed to assess the correlation of this variable.

(Fig. 3). Again, this was mostly evident on north-facing slopes as can be seen in Fig. 4F. Spatially, zones of more intense erosion and deposition are also observed in the main drainage lines.

Longer term monitoring periods integrate over such event-scale changes. Fig. 4G shows the observed topographic changes between the first and last event scale survey (119 days, i.e. LT1). The changes are very similar to those in ES1, though the area of erosion has expanded. The dominant effect of aspect is evident. These observations show as processes in sub-humid badlands are more weathering driven than in semi-arid landscapes where rainfall and overland flows are considered as the main drivers. Erosion was present in 42% of the area above the minLoD while deposition still is the dominant process in extent (58%, Table 2). The magnitude of the rates was similar yielding a net balance of 0.008 m (Table 2). These patterns are clearly affected by the event-scale processes observed in ES1 (Fig. 4B). Once the temporal scale increases, the effect of event-scale processes to longer term scales decreases. Fig. 4H presents observed changes at an annual scale (369 days; LT2) in the year preceding the event-scale surveys. Significant topographic changes are evident over 90% of the surface area. Intense erosion is observed on all the hillslopes (87% of the area above the minLoD) with a clear zone of deposition visible in the main drainage lines. A net rate of −0.062 m was observed. In this case deposition extent is reduced as the temporal scale increases and erosion becomes the dominant process. Fig. 4I shows the change over the total survey period (i.e. integrating the annual survey interval with all event-scale intervals; a total of 488 days). In this case (LT3) the 91% of the total badland area was above the minLoD, with erosion the dominant process (92%). The average erosion rate was −0.065 m; only 8% of the surface above the minLoD demonstrated deposition and the net balance for this interval was −0.054 m (Table 2). These results show as the dominant processes may change substantially based on the temporal scale in which these are observed. At annual temporal scales (or longer, LT2 and LT3) the effect of aspect in the sign of the topographic change is removed and the badland suffers majority degradation in all slopes, being deposition only concentrated in concave parts near the outlet of the badland (Fig. 4).

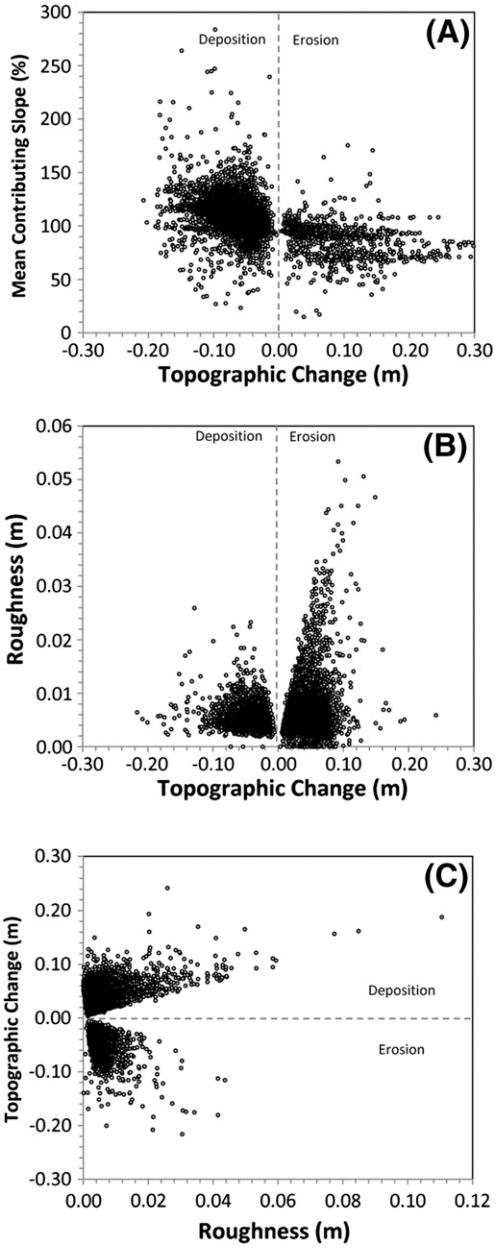

Fig. 5. Relationships between topographic change and (A) mean contributing slope (%) and (B) roughness (m) for LT 3 and ES1 respectively. The dependency of the minimum level of detection (minLoD) is responsible for the absence of data in the central part of the diagrams. In order to investigate the possible influence of the cells below the minLoD on the relationship in B an additional diagram was elaborated: (C) Relationship between roughness extracted from the DEM of the end of the interval and topographic change for ES1 period. Note that (a) the grey dashed line represents no-change, and erosion and deposition zones are indicated for reference; and (b) erosion reflects elevation decrease during the survey interval which may actually be related to erosional or shrink processes, while sedimentation reflects elevation increases which may actually reflect both depositional and dilatation processes.

4.2. Relationships between spatial patterns and topographic variables

For all cells where observed topographic change was above the threshold minimum level of detection (DoD > minLoD), topographic variables were analysed for statistical relationships with observed elevation changes in each survey interval. Pearson correlation coefficients are presented in Table 3; however, circular statistics (Berens, 2009) were used to assess the influence of aspect. The most significant topographic factors for each survey interval are highlighted in bold.

For all survey intervals aspect was significantly related to topographic change ($p < 0.01$) and was the most significant factor for ES1 and ES4. For ES2, ES3 and ES5 surface roughness is the most significant topographic variable, even more so when absolute changes are considered. The correlation value for this transformed variable (i.e. absolute topographic change) is presented in parentheses in the roughness column of Table 3. Slope also displays strong negative correlations with topographic change (ES3 and ES4) with steeper areas eroding more. Although statistically significant for some intervals, neither upstream area nor the topographic wetness index were the most significant predictor of topographic change in any survey interval.

Over longer timescales, aspect (LT1 and LT2) and mean contributing slope (LT3) are the most significant predictors of topographic change. As seen at the event-scale, steeper slopes led to preferential erosion. This relationship is presented in more detail in Fig. 5A for the period LT3 where the long-term effect of the mean contributing slope on topographic change is evident. Deposition is extremely rare on slopes > 100% and erosion increases with increasing slope angle.

From Table 3 it is apparent that roughness is correlated significantly with absolute topographic change for each survey interval, both at the event-scale and longer-term. An example of such a relationship (ES1) is presented in Fig. 5B. To confirm that the implementation of a roughness-dependent threshold minimum level of detection has not influenced this relationship, the statistical analysis was re-run on the raw non-thresholded DEMs for ES1. Results ($r = 0.15$, $p < 0.01$) demonstrate the minLoD has not a direct influence on this observed pattern. Rough areas appear to experience preferential topographic change in either direction. For example, over ES1 and ES2, deposition was dominant and roughness is a significant topographic predictor. However, during

Table 4
Pearson correlation coefficients between roughness and observed topographic changes at multiple temporal scales. Roughness was calculated form the DEM of the start of the interval and from the DEM of the end of the interval. Correlations for the absolute topographic changes are also represented. Significant correlations are indicated with one ($p < 0.01$) or two ($p < 0.05$) asterisks, while the strongest relationship for each survey period is also highlighted in bold.

Period	Number of observations	Roughness from DEMs of the start of the interval		ROUGHNESS from DEMs of the end of the interval	
		Topographic Change	Absolute Topographic Change	Topographic Change	Absolute Topographic Change
ES1	10975	0.098*	0.149*	0.105*	**0.360***
ES2	1738	0.242*	**0.687***	0.157*	0.575*
ES3	2323	−0.417*	**0.632***	−0.354*	0.543*
ES4	9592	0.067*	0.446*	−0.042*	**0.563***
ES5	6081	−0.005	**0.532***	−0.257*	0.383*
LT1	10800	0.095*	0.173*	0.020**	**0.237***
LT2	12664	−0.208*	**0.249***	−0.140*	0.165*
LT3	12800	−0.069*	0.105*	**−0.186***	0.172*

* $p < 0.01$, ** $p < 0.05$.

periods of net erosion (LT2, LT3), rougher areas also preferentially eroded.

The relationship in Fig. 5B represents the correlation between the roughness obtained from the DEM of the start of the survey interval and the subsequent topographic change. Further analysis examined whether a process-form feedback between roughness and topographic change could be detected by testing for a relationship between the observed topographic change and the roughness at the end of each interval. Table 4 shows the Pearson correlation coefficients for both roughness maps obtained from the DEMs of the start and the end of the intervals. The table also shows the correlation coefficients for the absolute topographic change. All periods show significant ($p < 0.01$) correlations whichever the DEM used to extract roughness. Fig. 5C demonstrates the relationship between roughness extracted from the DEM of the end of the interval and topographic change for the period ES1. The pattern observed is similar to that obtained for the initial roughness condition (Fig. 5B). These results suggest that rougher cells are indicative of more active topographic change and that they also are more likely to experience further topographic change in a process-form feedback. The limiting factors that prevent this positive feedback from perpetually self-reinforcing remain unclear.

4.3. Relationships between temporal variability and meteorological variables

Although only five event-scale survey intervals were available, a preliminary analysis to test for relationships between meteorological variables and hillslope-scale topographic change was conducted. Pearson correlations between the five meteorological variables and mean erosion and deposition, erosion and deposition areas and the overall sediment balance do not show significant correlation at the hillslope scale and, consequently, no further inferences are made herein.

4.4. Effects of spatial and temporal survey resolution

The effect of the spatial survey resolution was analysed based on two intervals. For one event-scale interval (ES1) and one long-term interval (LT3) the topographic change detection procedure was repeated at multiple grid scales and summary statistics analysed. ToPCAT was applied at 0.05, 0.10, 0.20, 0.50 and 1 metre grid sizes. Cell-statistics were calculated and the minimum level of detection was updated for each grid size. Fig. 6A and B compares the observed topographic change of DoDs for each grid size. Erosion, sedimentation and net changes are presented. At the event-scale (Fig. 6A), both observed erosion and deposition decrease as fewer cells display topographic changes greater than sub-grid topographic variability as grid size increase. Sub-grid roughness increases because topographic variability that was explicitly represented in the 50 mm DEM is now parameterised as sub-grid variability in a coarser grid and considered to be error in the topographic model. The net deposition observed in this period is gradually reduced with increasing grid size, demonstrating the importance of grid size for the estimation of sediment budgets in complex landscapes such badlands. Similar patterns are observed at the longer-term scale (Fig. 6B). The magnitude of the changes is similar for relatively small grid sizes (0.05–0.10 m). However, results for grid-sizes of 0.20 m differ slightly from those of the smaller scales, and differences are exacerbated when grid-size increases further to 0.5 m.

The importance of temporal survey frequency on calculated erosion and deposition volumes (and net change) was also analysed, considering only the data obtained during the intense survey period (1st September–29th December 2010) (Fig. 6C). Intermediate surveys were gradually removed from the analysis. Therefore, 5 scenarios were obtained containing from just 1 monitoring event-scale interval to 5 intervals. The inter-event effect of cancelling out topographic changes with subsequent topographic changes in the opposite direction is observed clearly as total observed erosion and deposition volumes decrease with a reduction in survey frequency. Effects on the net topographic change are less significant because erosion and deposition are affected to the same degree.

5. Discussion

In contrast to many more conventional and invasive methods to estimate erosion and deposition volumes in rapidly eroding landscapes, the morphometric method is capable of providing fully distributed estimates of topographic change thereby elucidating fine-scale spatial patterns of change. This can potentially provide substantial insight into both the quantities of sediment exported from a given area but also the controls and drivers of such geomorphic change. Terrestrial Laser Scanning (TLS) data sets may provide the required information for those estimates. Moreover, the non-contact nature of TLS removes problematic complications of surface disturbance when using 'invasive' methods such as erosion pins.

From the relationships identified between spatial patterns of topographic change and topographic variables in Table 3, three key factors emerge. First, a significant relationship between aspect and topographic change was evident for all survey intervals. For one interval in particular (ES1, Fig. 4B), this was the main driver of change. Aspect may control not just the sign of the change (e.g. ES1) but also its magnitude (e.g. LT1). Aspect has been observed to be an important factor in the development of sub-humid badlands (see early work by Churchill, 1981 or more recently Calvo-Cases and Harvey, 1996; Descroix and Olivry, 2002; Pulice et al., 2013) and, from the multi-temporal perspective provided here, this may be especially important at particular times of year (i.e. the first heavy rainfall event after a dry summer; the first frost event). Second, the relationship between slope and erosion (Fig. 5A) was also important, with a maximum threshold for deposition of 100% slope clearly evident (the influence of the slope angle on controlling

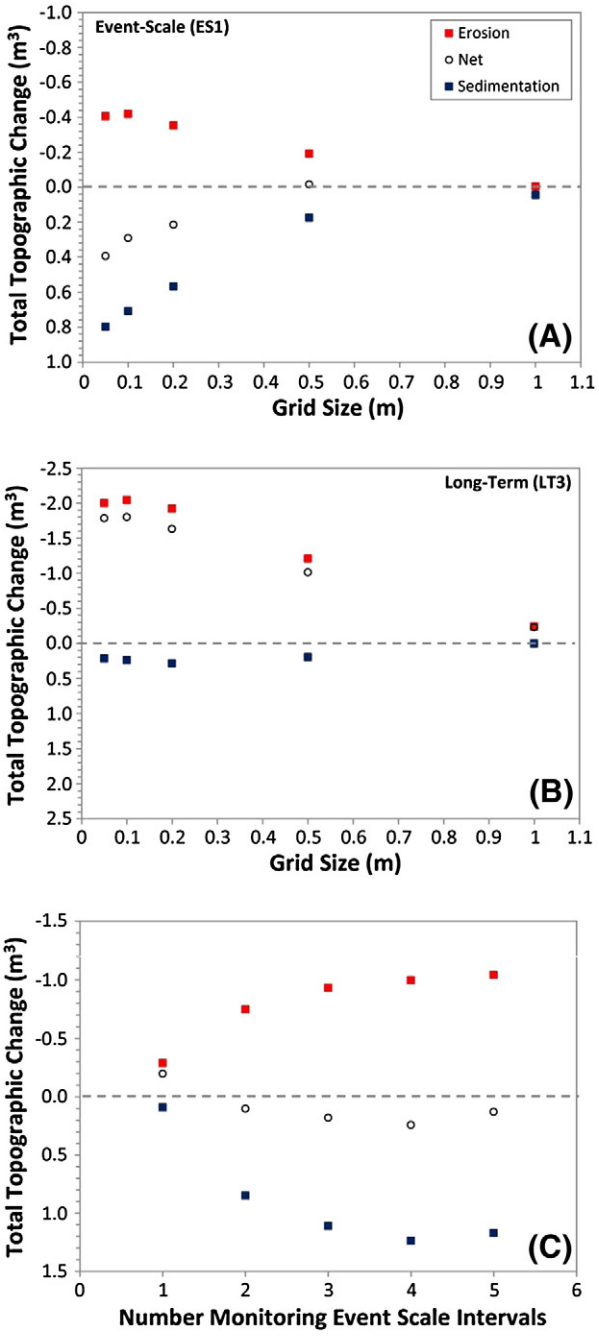

Fig. 6. The effect of spatial and temporal scale on sediment budgets. Variation of total erosion and deposition volumes (and net change) observed with grid size for both (A) event-scale (ES1) and (B) long-term monitoring (LT3) periods. (C) Variation of total erosion and deposition volumes (and net change) observed with number of surveys. Surveys obtained during the event-scale period are considered (1st September–29th December 2010; see Table 1 for more details). Intermediate surveys were gradually removed from the analysis. Legend is just represented in A but remains the same for all diagrams.

erodibility in badlands was early simulated by Cerdá and García-Fayos, 1997).

Third, a significant linear relationship between absolute topographic change and surface roughness was observed consistently throughout the monitoring campaign. The importance of roughness is highlighted because of the event-scale surveys conducted in this study. Over longer timescales, the relationship is less pronounced as slope becomes relatively more important. This is an interesting finding as it suggests that important process-form feedbacks are taking place at event-scales; yet, when monitoring takes place at an annual scale, dynamic, rapidly evolving roughness is not detected. Long-term topographic changes are related to initial roughness less strongly because roughness changes soon after the initial survey. Thus, the important control of surface roughness on geomorphic processes in highly erodible badlands may be overlooked in long-term surveys.

A comparison of summary statistics of topographic change and meteorological variables yielded no significant relationships. The small number of event-scale intervals (a total of five) meant that any relationships would be rather tentative and could explain the absence of significant relationships. An alternative interpretation is that the diversity of geomorphic processes operating in the badland (e.g. interrill and rill erosion/deposition, aeolian erosion and deposition, shrink-swelling and frost expansion) obscures any such relationship when the resultant topographic change from all of these processes is aggregated across survey areas.

When analysing morphometric sediment budgets, a number of important factors must be considered. First is the error associated with each individual topographic model and the need to propagate this error into the resulting DoD. Without robust error analysis, estimated erosion/deposition rates will be dominated by supposed small-scale changes observed throughout the study area that are, in fact, an artefact of measurement error and need to be considered uncertain. This approach has been applied widely in fluvial studies as the early work by Brasington et al. (2000, 2003) showed. Following Wheaton et al. (2010), this study applied a spatially variable minimum level of detection to each grid cell separately, calculated from the detrended standard deviation of elevations within each cell. Thus, where observed topographic changes within a grid cell are substantially larger than the topographic variability within that cell, the observation is more reliable. With that in mind, the use of detrended standard deviation of elevations appears to be appropriate in this setting. Other errors (e.g. registration and georeferencing errors) were substantially (i.e. an order of magnitude) below the grid size and minimum level of detection applied. Data quality is critical if observed changes are to be reliably attributed to real geomorphic change. For example, the aspect-driven pattern of erosion and deposition in ES1 (Fig. 4B) is similar to that expected from misalignment of subsequent scans during the registration process. Yet, from the survey methods and errors described, geomorphic changes can be distinguished from such errors with confidence. This is further supported by elimination of aspect-variability over annual scale surveys (Fig. 4H–I).

The second main consideration is the temporal scale of measurement. Comparison of consecutive event-scale surveys alongside longer-term survey intervals that integrate over multiple events reveals different patterns. In this particular study, the main topographic change was observed in a single event-scale interval when intense rainfall was observed. However, several changes observed at the event-scale were cancelled out by further topographic changes in the opposite direction (i.e. erosion followed by deposition) that cannot be discerned from longer monitoring intervals. When attempting to determine the geomorphic effectiveness of meteorological and hydrological processes, an event-scale survey resolution is clearly important or else real changes will not be detected. The stronger control of roughness observed at the event-scale exemplifies the importance of event-scale monitoring.

Third, in badland environments subject to substantial seasonal variability in both rainfall and temperature, the timing of surveys is an important consideration when establishing long-term erosion rates. Shrink-swelling and freeze-thaw processes may cause dilation of surface material which results in a net surface elevation increase (Fig. 4B and Table 2). Survey intervals that stretch over seasonal transitions without incorporating a full annual cycle (e.g. net deposition from September to December in Fig. 4G) may be dominated by such temporary changes that will ultimately be reversed in the full annual cycle (e.g. net erosion in Fig. 4H–I). This could potentially bias estimated long-term erosion rates derived from morphometric surveys.

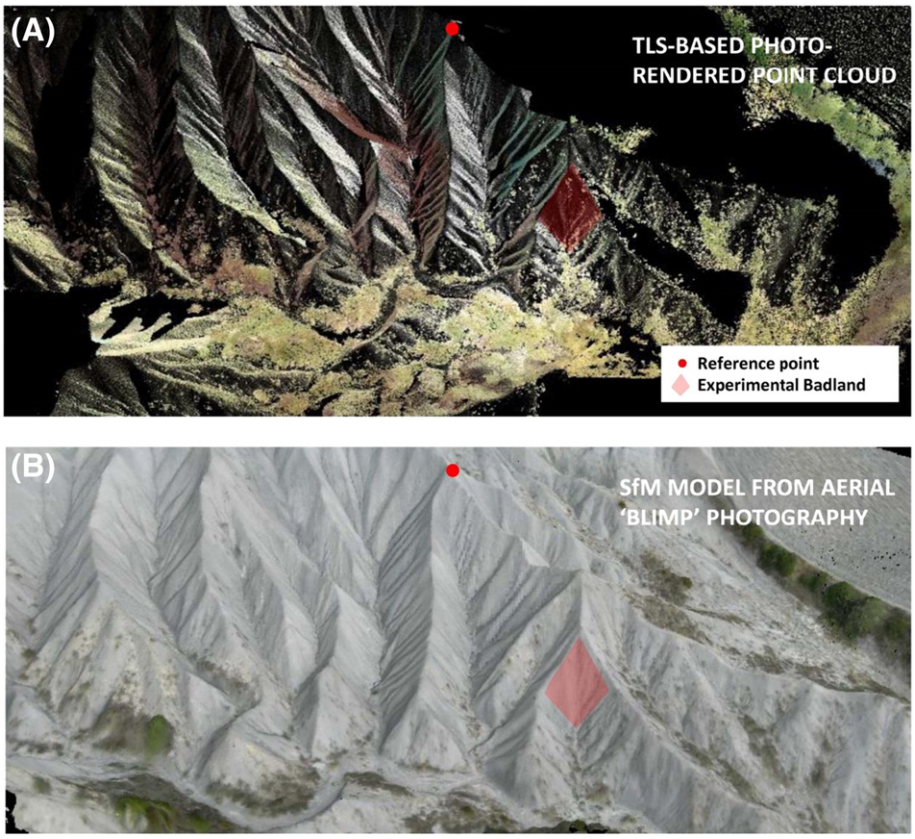

Fig. 7. Potential to upscale morphometric method of sediment transport to examine landscape-scale controls on sediment transport and connectivity. (A) Example landscape-scale TLS point cloud (note: further TLS stations would reduce visible occlusions). (B) Photo-rendered topographic model of the same location using Structure-from-Motion (SfM) on aerial (blimp) imagery to acquire topographic data at the landscape scale. The location of the experimental badland of this study is indicated in both images.

Fourth, the spatial resolution of both topographic data acquisition and terrain product resolution is critical to the calculated sediment budgets. This is demonstrated clearly in Fig. 6. Without high-resolution topographic data small changes would not be discerned and both erosion and deposition would be underestimated. In our case, sub-grid point densities of 5 points cm^{-2} on average have been obtained to extract the terrain products. The spatial resolution of the final DoD will ultimately be limited by available data density and precision. The effect of spatial resolution on calculated sediment budgets requires further investigation.

Finally, the results herein highlight the need for concurrent process observations to distinguish between mechanisms of topographic change. At present, we are unable to differentiate between erosion-sedimentation from shrink-swelling processes. Meteorological observations lend support to present interpretations, but further instrumentation and an analysis of soil physico-chemical characteristics would be necessary to confirm such interpretations. For example, it is possible that the uniform and widespread erosion in ES4 (Fig. 4E) is the result of either aeolian or runoff entrainment or simply the reversal of surface material expansion processes. The ability to distinguish between erosion mechanisms with confidence would add great value to the data products resulting from multi-temporal surveys and would help to develop more specific relationships with meteorological variables. Further investigation of sub-grid roughness parameterisations could potentially identify roughness parameters that are able to distinguish reliably each of these mechanisms, yielding a substantial advance in our process knowledge. This represents an important avenue of further research.

Although the workflow outlined in this pilot study was only applied to a relatively small area, it is easily upscaled to larger areas. Indeed, survey technology has advanced substantially in the last few years alone with the latest generation of TLS devices capable of data acquisition rates at least two orders of magnitude greater than the instrumentation used here. Moreover, the maximum range of terrestrial laser scanners is now > 1 km. With careful survey design, the method presented here can be upscaled readily from the hillslope scale to cover entire badland systems. Such surveys permit detailed analysis of controls of sedimentological connectivity across badlands. Fig. 7A presents an example of this enhanced capability using only a small number of registered TLS surveys. With a larger number of TLS stations, shadowing effects can be minimised across large areas. A follow-up monitoring study covering an area of ~5000 m^2 is currently underway in a new experimental sub-humid badland. Other developments include the recent emergence of 'Structure-from-Motion' (SfM) survey techniques that enable the rapid generation of dense topographic models using imagery from consumer-grade digital cameras which can then be georeferenced (Fig. 7B). The reliability and precision of this novel technique is the focus of recent and on-going research (Fonstad et al., 2013; James and Robson, 2012; Westoby et al., 2012). Further evaluation of the change-detection capabilities of multi-temporal SfM surveys is also underway. Certainly, development of this low-cost survey technique alongside the proliferation of budget unmanned aerial vehicles (UAVs; Carrivick et al., 2013; Vericat et al., 2009) could expand considerably the accessibility of morphometric sediment budgets in a variety of geomorphic settings.

6. Concluding remarks

The high quantities of sediment exported from erodible badlands emphasises the importance of establishing both accurate sediment budgets for these areas, but also of understanding the processes responsible for this high level of erosion. The application of TLS and other high-resolution survey methods to detect topographic change in highly

erodible badlands has considerable potential. A pilot application of this nascent technique of badland monitoring is presented. Topographic controls on spatial patterns of erosion and deposition can be elucidated from event-scale multi-temporal surveys. Aspect, surface roughness and slope are especially significant predictors of topographic change. In particular, it appears that surface roughness is proportionately more important at controlling badland geomorphological processes at the event-scale than can be discerned from longer-scale monitoring. This may have led to longer-term studies underestimating the importance of surface roughness as a geomorphological control. Increased availability of high resolution topographic data means that analysis of surface roughness is likely to become more important to future analyses of geomorphic controls.

Acknowledgements

This research has been carried out within the framework of the Research Project BadlandScan, funded by the Spanish Institute of Altoaragoneses Studies (Instituto de Estudios Altoaragoneses, Diputación de Huesca). The first author has a Ramon y Cajal Fellowship (RYC-2010-06264) funded by the Spanish Ministry. The second author received an early-career grant from the British Society for Geomorphology which assisted the completion of this manuscript. The support of the members of the Fluvial Dynamics Research Group and Chris Gibbins is greatly appreciated. We also appreciate the kindness of the landowner, and the support of the Water Ebro Authorities and locals. Finally, research in the Isábena and Ésera basins (background data, general patterns) has been carried out within the framework of the projects SESAM, funded by the German Science Foundation (Deutsche Forschungsgemeinschaft, DFG), and SCARCE (Consolider Ingenio 2010 CSD2009-00065) funded by the Spanish Ministry of Economy and Competitiveness.

References

Alatorre, L.C., Beguería, S., García-Ruiz, J.M., 2010. Regional scale modelling of hillslope sediment delivery: a case study in Barasona reservoir watershed (Spain) using WATEM/SEDEM. J. Hydrol. 391, 109–123.

Alexander, R.W., Harvey, A.M., Calvo, A., James, P.A., Cerdà, A., 1994. Natural stabilisation mechanisms on badland slopes: Tabernas, Almeria, Spain. In: Millington, A.C., Pye, K. (Eds.), Environmental change in drylands: biogeographical and geomorphological perspectives. Wiley, Chichester, pp. 85–111.

Ashmore, P., Church, M., 1998. Sediment transport and river morphology: a paradigm for study. In: Klingeman, P.C., Beschta, R.L., Komar, P.D., Bradley, J.B., Klingeman, P.C., Beschta, R.L., Komar, P.D., Bradley, J.B., Klingeman, P.C., Beschta, R.L., Komar, P.D., Bradley, J.B. (Eds.), Gravel Bed Rivers in the Environment. Water Resources Publications, Highlands Ranch, CO, pp. 115–148.

Avendaño, C., Sanz, M.E., Cobo, R., 2000. State of the art of reservoir sedimentation management in Spain. Proceedings of the International Workshop and Symposium on Reservoir Sedimentation Management, Tokyo, Japan, pp. 27–35.

Ballesteros-Cánovas, J.A., Bodoque, J.M., Lucía, A., Martín-Duque, J.F., Díez-Herrero, A., Ruiz-Villanueva, V., Rubialesd, J.M., Genova, M., 2013. Dendrogeomorphology in badlands: Methods, case studies and prospects. Catena 106, 113–122.

Berens, P., 2009. CircStat: A Matlab Toolbox for Circular Statistics. J. Stat. Softw. 31 (10), 1–21.

Boardman, J., 2006. Soil erosion science: reflections on the limitations of current approaches. Catena 68, 73–86.

Boix-Fayos, C., Martinez-Mena, M., Arnau-Rosalen, E., Calvo-Cases, A., Castillo, V., Albaladejo, J., 2006. Measuring soil erosion by field plots: understanding the sources of variation. Earth Sci. Rev. 78, 267–285.

Brasington, J., Smart, R.M.A., 2003. Close range digital photogrammetric analysis of experimental drainage basin evolution. Earth Surf. Process. Landf. 28, 231–247.

Brasington, J., Rumsby, B.T., McVey, R.A., 2000. Monitoring and modelling morphological change in a braided gravel-bed river using high resolution GPS-based survey. Earth Surf. Process. Landf. 25, 973–990.

Brasington, J., Langham, J., Rumsby, B., 2003. Methodological sensitivity of morphometric estimates of coarse fluvial sediment transport. Geomorphology 53, 299–316.

Brasington, J., Vericat, D., Rychkov, I., 2012. Modeling river bed morphology, roughness, and surface sedimentology using high resolution terrestrial laser scanning. Water Resour. Res. 48, 1–18.

Bretar, F., Chauve, A., Bailly, J.-S., Mallet, C., Jacome, A., 2009. Terrain surfaces and 3-D landcover classification from small footprint full-waveform lidar data: application to badlands. Hydrol. Earth Syst. Sci. 13, 1531–1544.

Bryan, R., Yair, A., 1982. Perspectives on studies of badland geomorphology. In: Bryan, R., Yair, A. (Eds.), Badland Geomorphology & Piping. Geo Books, Cambridge, pp. 1–12.

Buendia, C., Gibbins, C.N., Vericat, D., Batalla, R.J., 2013. Reach and catchment-scale influences on invertebrate assemblages in a river with naturally high fine sediment loads. Limnol. Ecol. Manag. Inland Waters 43 (5), 362–370.

Calvo-Cases, A., Harvey, A.M., 1996. Morphology and development of selected badlands in southeast Spain: Implications of climatic change. Earth Surf. Process. Landf. 21, 725–735.

Cantón, Y., Domingo, F., Solé-Benet, A., Puigdefábregas, J., 2001. Hydrological and erosion response of a badlands system in semiarid SE Spain. J. Hydrol. 252, 65–84.

Cantón, Y., Solé-Benet, A., Domingo, F., 2004. Temporal and spatial patterns of soil moisture in semiarid badlands of SE Spain. J. Hydrol. 285, 199–214.

Cantón, Y., Solé-Benet, A., de Vente, J., Boix-Fayos, C., Calvo-Cases, A., Asensio, C., Puigdefábregas, J., 2011. A review of runoff generation and soil erosion across scales in semiarid south-eastern Spain. J. Arid Environ. 75, 1254–1261.

Carrivick, J.L., Smith, M.W., Quincey, D.J., Carver, S.J., 2013. Developments in budget remote sensing for the geosciences. Geol. Today 29, 138–143.

Cerdà, A., 2002. The effect of season and parent material on water erosion on highly eroded soils in eastern Spain. J. Arid Environ. 52, 319–337.

Cerdá, A., García-Fayos, P., 1997. The influence of slope angle on sediment, water and seed losses on badland landscapes. Geomorphology 18 (2), 77–90.

Churchill, R.R., 1981. Aspect-Related Differences in Badlands Slope Morphology. Ann. Assoc. Am. Geogr. 71 (3), 374–388.

Ciccacci, S., Galiano, M., Roma, M.A., Salvatore, M.C., 2008. Morphological analysis and erosion rate evaluation in badlands of Radicofani area (southern Tuscany – Italy). Catena 74, 87–97.

Clarke, M.L., Rendell, H.L., 2006. Process-form relationships in Southern Italian badlands: Erosion rates and implications for landform evolution. Earth Surf. Process. Landf. 31, 15–29.

Clarke, M.L., Rendell, H.M., 2010. Climate-driven decrease in erosion in extant Mediterranean badlands. Earth Surf. Process. Landf. 35, 1281–1288.

Della Seta, M., Del Monte, M., Fredi, P., Lupia-Palmieni, E., 2009. Space-time variability of denudation rates at the catchment and hillslope scales on the Tyrrhenian side of Central Italy. Geomorphology 107, 161–177.

Descroix, L., Claude, J.C., 2002. Spatial and temporal factors of erosion by water of black marls in the badlands of the French southern Alps. Hydrol. Sci. J. 47, 227–242.

Descroix, L., Olivry, J.C., 2002. Spatial and temporal factors of erosion by water of black marls in the badlands of the French Southern Alps. Hydrol. Sci. J. 47 (2), 227–242.

Desir, G., Marín, C., 2007. Factors controlling the erosion rates in a semi-arid zone (Bardenas Reales, NE Spain). Catena 71, 31–40.

Eitel, J.U.H., Williams, C.J., Vierling, L.A., Al-Hamdan, O.Z., Pierson, F.P., 2011. Suitability of terrestrial laser scanning for studying surface roughness effects on concentrated flow erosion processes in rangelands. Catena 87 (3), 398–407.

Fairbridge, R.W., 1968. The Encyclopedia of Geomorphology. Reinhold Book Corp, New York p. 1275.

Fargas, D., Martínez-Casasnovas, J.A., Poch, R., 1997. Identification of critical sediment source areas at regional level. Phys. Chem. Earth 22, 355–359.

Faulkner, H., 2008. Connectivity as a crucial determinant of badland morphology and evolution. Geomorphology 100, 91–103.

Faulkner, H., Spivey, D., Alexander, R., 2000. The role of some site geochemical processes in the development and stabilisation of three badland sites in Almería, Southern Spain. Geomorphology 35, 87–99.

Fonstad, M.A., Dietrich, J.T., Courville, B.C., Jensen, J.L., Carbonneau, P.E., 2013. Topographic structure from motion: a new development in photogrammetric measurement. Earth Surf. Process. Landf. 38, 421–430.

Francke, T., 2009. Measurement and modelling of water and sediment fluxes in mesoscale dryland catchments. Ph.D. Thesis Universität Potsdam, Germany.

Francke, T., López-Tarazón, J.A., Vericat, D., Bronstert, A., Batalla, R.J., 2008. Flood-based analysis of high-magnitude sediment transport using a non-parametric method. Earth Surf. Process. Landf. 33, 2064–2077.

Fuller, I.C., Marden, M., 2011. Slope-channel coupling in steepland terrain: A field-based conceptual model from the Tarndale gully and fan, Waipaoa catchment, New Zealand. Geomorphology 128, 105–115.

Gallart, F., Marignani, M., Pérez-Gallego, N., Santi, E., Maccherini, S., 2013. Thirty years of studies on badlands, from physical to vegetational approaches. A succinct review. Catena 106, 4–11.

García-Ruiz, J.M., Regüés, D., Alvera, B., Lana-Renault, N., Serrano-Muela, P., Nadal-Romero, E., Navas, A., Latron, J., Martí-Bono, C., Arnáez, J., 2008. Flood generation and sediment transport in experimental catchments affected by land use changes in the central Pyrenees. J. Hydrol. 356, 245–260.

Godfrey, A.E., Everitt, B.L., Martín Duque, J.F., 2008. Episodic sediment delivery and landscape connectivity in the Mancos Shale badlands and Fremont River system, Utah, USA. Geomorphology 122, 242–251.

Howard, A.D., 1994. Badlands. In: Abrahams, A., Parsons, A. (Eds.), Geomorphology of Desert Environments. Chapman and Hall, London, pp. 213–242.

Imeson, A.C., Kwaad, F.J.P.M., Verstraten, J.M., 1982. The relationship of soil physical and chemical properties to the development of bandlands in Morocco. In: Bryan, R., Yair, A. (Eds.), Badland Geomorphology & Piping. Geo Books, Cambridge, pp. 47–70.

James, M.R., Robson, S., 2012. Straightforward reconstruction of 3D surfaces and topography with a camera: accuracy and geoscience application. J. Geophys. Res. 117, F03017. http://dx.doi.org/10.1029/2011JF002289.

Kasanin-Grubin, M., 2013. Clay mineralogy as a crucial factor in badland hillslope processes. Catena 106, 54–67.

Kuhn, N.J., Yair, A., 2004. Spatial distribution of surface conditions and runoff generation in small arid watersheds, Zin Valley Badlands, Israel. Geomorphology 57, 183–200.

Lane, S.N., Chandler, J.H., 2003. Editorial: The generation of high quality topographic data for hydrology and geomorphology: new data sources, new applications and new problems. Earth Surf. Process. Landf. 28, 229–230.

Lázaro, R., Cantón, Y., Solé-Benet, A., Bevan, J., Alexander, R., Sancho, L.G., Puigdefábregas, J., 2008. The influence of competition between lichen colonization and erosion on the evolution of soil surfaces in the Tabernas badlands (SE Spain) and its landscape effects. Geomorphology 102, 252–266.
Liu, X., 2008. Airborne LiDAR for DEM generation: some critical issues. Prog. Phys. Geogr. 32 (1), 31–49.
Lopez-Saez, J., Corona, C., Stoffel, M., Rovéra, G., Astrade, L., Berger, F., 2011. Mapping of erosion rates in marly badlands based on a coupling of anatomical changes in exposed roots with slope maps derived from LiDAR data. Earth Surf. Process. Landf. 36, 1162–1171.
López-Tarazón, J.A., Batalla, R.J., Vericat, D., 2011. In-channel sediment storage in a highly erodible catchment: the River Isábena (Ebro Basin, Southern Pyrenees). Z. Geomorphol. 55 (3), 365–382.
López-Tarazón, J.A., Batalla, R.J., Vericat, D., Francke, T., 2012. The sediment budget of a highly dynamic mesoscale catchment: The River Isábena. Geomorphology 138, 15–28.
Lucía, A., Martín-Duque, J.A., Laronne, J.B., Sanz-Santos, M.A., 2011a. Geomorphic dynamics of gullies developed in sandy slopes of Central Spain. Landf. Anal. 17, 91–97.
Lucía, A., Laronne, J.B., Martín-Duque, J.A., 2011b. Geodynamic processes on sandy slope gullies in central Spain field observations, methods and measurements in a singular system. Geodin. Acta 24 (2), 61–79.
Milan, D.J., Heritage, G.L., Hetherington, D., 2007. Application of a 3D laser scanner in the assessment of erosion and deposition volumes and channel change in a proglacial river. Earth Surf. Process. Landf. 32, 1657–1674.
Nadal-Romero, E., Regüés, D., Martí-Bono, C., Serrano-Muela, P., 2007. Badland dynamics in the Central Pyrenees: temporal and spatial patterns of weathering processes. Earth Surf. Process. Landf. 32, 888–904.
Nadal-Romero, E., Martínez-Murillo, J.F., Vanmaercke, M., Poesen, J., 2011. Scale-dependency of sediment yield from badland areas in Mediterranean environments. Prog. Phys. Geogr. 35, 297–332.
Nadal-Romero, E., Torri, D., Yair, A., 2013. Updating the badlands experience. Catena 106, 1–3.
Palau, A., 1998. Estudio limnológico del ecosistema fluvial afectado por los vaciados del embalse de Barasona. Limnética 14, 1–15.
Pulice, I., Di Leob, P., Robustellia, G., Scarcigliaa, F., Cavalcanteb, F., Belvisob, C., 2013. Control of climate and local topography on dynamic evolution of badland from southern Italy (Calabria). Catena 109, 83–95.
Regüés, D., Gallart, F., 2004. Seasonal patterns of runoff and erosion responses to simulated rainfall in a badland area in Mediterranean mountain conditions (Vallcebre, Southeastern Pyrenees). Earth Surf. Process. Landf. 29, 755–767.
Regüés, D., Nadal-Romero, E., 2013. Uncertainty in the evaluation of sediment yield from badland areas: Suspended sediment transport estimated in the Araguás catchment (central Spanish Pyrenees). Catena 106, 93–100.
Rychkov, I., Brasington, J., Vericat, D., 2012. Computational and methodological aspects of terrestrial surface analysis based on point clouds. Comput. Geosci. 42, 64–70.
Schumm, S.A., 1956. Evolution of drainage systems and slopes in badlands at Perth Amboy, New Jersey. Geol. Soc. Am. Bull. 67, 597–645.
Sirvent, J., Desir, G., Gutiérrez, M., Sancho, C., Benito, G., 1997. Erosion rates in badland areas recorded by collectors, erosion pins and profilometer techniques (Ebro Basin, NE-Spain). Geomorphology 18, 61–75.
Solé-Benet, A., Calvo, A., Cerdà, A., Lázaro, R., Pini, R., Barbero, J., 1997. Influence of micro-relief patterns and plant cover on runoff related processes in badlands from Tabernas (SE Spain). Catena 31, 23–38.
Thommeret, N., Bailly, J.S., Puech, C., 2010. Robust extraction of thalwegs network from DTM: application on badlands. Hydrol. Earth Syst. Sci. 7, 879–905.
Torri, D., Regüés, D., Pellegrini, S., Bazzoffi, P., 1999. Within-storm soil surface dynamics and erosive effects of rainstorms. Catena 38, 131–150.
Vergari, F., Della Seta, M., Del Monte, M., Barbieri, M., 2013. Badlands denudation "hot spots": The role of parent material properties on geomorphic processes in 20-years monitored sites of Southern Tuscany (Italy). Catena 106, 31–41.
Vericat, D., Brasington, J., Wheaton, J., Cowie, M., 2009. Accuracy assessment of aerial photographs acquired using lighter-than-air blimps: low cost tools for mapping river corridors. River Res. Appl. 25, 985–1000.
Wainwright, J., Brazier, R.E., 2011. Slope systems, In: Thomas, D.S.G. (Ed.), Arid Zone Geomorphology: process, form and change in drylands, Third edition. John Wiley & Sons, Chichester, pp. 209–233.
Westoby, M.J., Brasington, J., Glasser, N.F., Hambrey, M.J., Reynolds, J.M., 2012. 'Structure-from-Motion' photogrammetry: A low-cost, effective tool for geoscience applications. Geomorphology 179, 300–314.
Wheaton, J.M., Brasington, J., Darby, S.E., Sear, D.A., 2010. Accounting for uncertainty in DEMs from repeat topographic surveys: improved sediment budgets. Earth Surf. Process. Landf. 35, 136–156.
Williams, R.D., Brasington, J., Vericat, D., Hicks, D.M., Labrosse, F., Neal, M.N., 2011. Monitoring braided river change using terrestrial laser scanning and optical bathymetric mapping. In: Smith, M., Paron, P., Griffiths, J. (Eds.), Geomorphological Mapping. Elsevier, Oxford, pp. 507–531.
Yair, A., Lavee, H., 1985. Runoff generation in arid and semi-arid zones. In: Anderson, M.G., Burt, T.P. (Eds.), Hydrological Forecasting. Wiley, Chichester, pp. 183–220.